Journal of
Materials Chemistry A

Highly H2O Permeable Ionic Liquid Encapsulated Metal-Organic Framework Membranes for Energy-efficient Air-Dehumidification

Journal:	*Journal of Materials Chemistry A*
Manuscript ID	TA-ART-08-2020-007780.R1
Article Type:	Paper
Date Submitted by the Author:	30-Sep-2020
Complete List of Authors:	Park, Sunghwan; Texas A&M University at College Station, Chemical Engineering Jeong, Hae-Kwon; Texas A&M University at College Station, Chemical Engineering

SCHOLARONE™
Manuscripts

ARTICLE

Highly H₂O Permeable Ionic Liquid Encapsulated Metal-Organic Framework Membranes for Energy-efficient Air-Dehumidification

Sunghwan Park[a] and Hae-Kwon Jeong*[ab]

Isothermal membrane-based air dehumidification (IMAD) is much more energy-efficient and economical than traditional air-dehumidification technologies. There are, however, no practical IMAD processes technologies currently available mainly due to limitations of current membranes. Ionic liquids (ILs) are a promising air-dehumidification membrane material. Current supported IL membranes suffer from poor stability, limiting their performances. Herein, we propose new stable IL membranes, encapsulated IL membranes (EILMs) by encapsulating 1-butyl-3-methylimidazolium bromide ([C₄MIM][Br]) into ultrathin polycrystalline UiO-66-NH₂ metal-organic framework membranes via a ship-in-a-bottle method. Stability of IL membranes is significantly enhanced due to the IL entrapped in the pore cages of UiO-66-NH₂. The EILMs show unprecedentedly high H₂O permeance (~ 2.36 x 10⁻⁴ mol m⁻² s⁻¹ Pa⁻¹), an order of magnitude greater than the most permeable air-dehumidification membranes reported so far. Furthermore, the encapsulated [C₄MIM][Br] drastically increase the H₂O/N₂ separation factor to ~ 1560, satisfying the minimally required H₂O/N₂ separation performance for commercially-viable air-dehumidification.

Introduction

Heating, ventilation, and air-conditioning (HVAC) systems have been critically important for our daily lives. However, more than 90 % of the current HVAC systems rely on an energy-intensive vapor compression system, consuming more than 76 % of total electricity and ~ 35 % of total energy annually in the U.S.[1] Also, the emission of synthetic refrigerants such as hydrofluorocarbons (HFCs) used in a vapor compression system accelerates global warming.[2] According to the U.S. Department of Energy (DOE), isothermal membrane-based air dehumidification (IMAD) is one of the most promising technologies for energy-efficient and eco-friendly HVAC.[3] In theory, an integrated IMAD and evaporative cooling system can reduce energy consumption by 86.2 % as compared to conventional vapor compression.[4]

Membranes of hygroscopic organic liquids such as triethylene glycol (TEG), polyethylene glycol (PEG), and ionic liquids (ILs) have been explored for energy-efficient air-dehumidification due to their superior hydrophilicities.[5-8] As compared to other hygroscopic liquids, ILs are known more stable due to their negligible vapor pressures as well as more versatile due to their tailorable properties by the diverse combinations of cations and anions. Current IL membranes (i.e., supported ionic liquid membranes (SILMs)), however, commonly suffer from their poor stability and limited performances.[9] In SILMs, ILs are impregnated by capillary force in macro/mesoporous supports, where the ILs can be leached out by pressurization, dissolution, evaporation, and etc.[10] Accordingly, the IL layers were generally made quite thick (> 10 μm) in order to suppress the loss of ILs.[9] Another way to form stable SILMs is to use ILs with high viscosity,[11] which then lower the diffusivity of water vapor. Furthermore, the separation performances of the SILMs impregnated with bulk ILs are likely limited by the slow diffusion of gas molecules from the gas/IL interfaces to the bulk ILs.[12] For example, ILs in contact with CO₂ at the interface were rapidly saturated with CO₂, resulting in a CO₂ saturated dense layer with strong CO₂-IL interactions.[12] Due to the strong interactions, CO₂ diffused slowly from the interface into bulk ILs, lowering the overall efficiency of CO₂ adsorption.[12]

In order to address above-mentioned challenges of supported IL membranes, there have been several efforts.[9, 13, 14] Bara et al.[15] prepared poly(ionic liquid) membranes by radical polymerization of IL monomers, showing improved mechanical stability. However, the polymerization decreased the separation performance of the membranes due to the restricted mobility of IL fragments.[14] Voss et al.[16] developed gelled IL membranes by forming networks of IL using low molecular-mass organic gelators. The membranes showed enhanced mechanical stability with preserved separation performances. Nevertheless, the gelled IL turned back into liquid with increasing temperature.[13] Friess et al.[17] reported polymer/IL mixed-matrix membranes (MMMs) exhibiting promising results. However, these MMMs suffered from limited IL concentration and phase separation due to the stability and the compatibility of IL.[13] It is, therefore, highly desirable to develop new strategies to fabricate IL membranes that can

a. Artie McFerrin Department of Chemical Engineering and b. Department of Materials Science and Engineering, Texas A&M University, 3122 TAMU, College Station, TX 77843-3122, United States.

overcome the trade-off between separation performance and stability.

One of the effective strategies to stabilize ILs is to use the composite of ILs with microporous materials such as metal-organic frameworks (MOFs).[18-20] For example, IL-encapsulated MOFs were found effective as catalysts,[21] sorbents,[22] fuel cell membranes,[23] desulfurization,[24] and gas separation membranes.[25, 26] There have been several preparation methods reported for IL/MOF composites which can be divided broadly into two categories: 1) ionothermal synthesis and 2) post-impregnation. In ionothermal synthesis, IL/MOF composites were prepared by *in-situ* synthesizing MOFs in IL as a solvent and structure-directing agent.[26] In contrast, post-impregnation methods are more straightforward since ILs were impregnated in preformed MOFs.[18, 19] One common post-impregnation method is wet impregnation, where IL diluted in a solvent is impregnated into MOFs followed by solvent removal.[27] Though this post-impregnation method is simple, leaching of ILs trapped in MOFs is a common issue. Another post-impregnation method is ship-in-a-bottle method where smaller IL precursors are impregnated and subsequently reacted to form bulkier ILs in MOF cages.[22] It is much less likely for the bulkier ILs encapsulated in the micropore cages of MOFs to leach even under harsh conditions.[22]

Here, we present a new class of supported IL membranes named encapsulated ionic liquid membranes (EILMs). EILMs were prepared by encapsulating IL in polycrystalline MOF membranes by a ship-in-a-bottle (SIB) strategy. We chose 1-butyl-3-methylimidazolium bromide ([C$_4$MIM][Br]) and UiO-66-NH$_2$ MOF membranes as IL and microporous supports, respectively. The EILMs were thoroughly characterized and the amounts of IL encapsulated were fully determined. The water vapor transport properties of the encapsulated IL were investigated in terms of water vapor sorption and diffusion. Lastly, the H$_2$O/N$_2$ separation performances of the EILMs and their stability were tested under various conditions.

Experimental

Materials

For UiO-66-NH$_2$ synthesis, zirconium (IV) chloride (ZrCl$_4$, > 99.5 %, Sigma Aldrich), 2-aminoterephthalic acid (H$_2$BDC-NH$_2$) (H$_2$NC$_6$H$_3$-1,4-(CO$_2$H)$_2$, 99%, Acros Organics), acetic acid (CH$_3$CO$_2$H, > 99.7 %, Alfa Aesar), and N,N-dimethylformamide (DMF) (HCON(CH$_3$)$_2$, > 99.8 %, Alfa Aesar) were used. For ionic liquid synthesis, 1-methylimidazole (1-MIM) (C$_4$H$_6$N$_2$, 99 %, Sigma Aldrich) and 1-bromobutane (C$_4$Br) (CH$_3$(CH$_2$)$_3$Br, 99 %, Sigma Aldrich) were used. All chemicals were used without further purifications.

Preparation of α-alumina supports

α-alumina supports were prepared by following a recipe reported previously.[28] In a typical preparation, 1.9 g of α-alumina powder (CR6, Baikowski) was homogeneously mixed with 0.2 ml of a polymer binder solution. The binder solution was prepared by dissolving 3 g of polyvinyl alcohol (PVA) (Mw: 22k, Duksan) in a mixture of 5 ml of 1 M HNO$_3$ and 95 ml of D.I.

water. An α-alumina disk was formed by pressing a mold filled with 2.1 g of the alumina/binder mixture uniaxially at 200 bar. Afterwards, the disk was sintered at 1100 °C for 2 hrs at the ramp rate of 5 °C min^{-1}. The sintered α-alumina disk was polished using a sandpaper (grid #1200). The prepared α-alumina disk was 2.2 cm in diameter, 2 mm in thickness, and 46 % porosity with an average pore diameter of ~ 200 nm.

Synthesis of UiO-66-NH$_2$ particles

UiO-66-NH$_2$ particles were synthesized solvothermally based on a recipe reported with a slight modification.[29] A precursor solution was prepared by mixing 0.301 g of ZrCl$_4$, 0.215 g of NH$_2$-BDC, and 11.63 g of acetic acid in 30 ml of DMF. The prepared solution was placed in a Teflon-lined autoclave. Solvothermal reaction was carried out at 120 °C for 48 hrs in a convection oven. After completion of the reaction, the autoclave was naturally cooled down at room temperature for 2 hrs. The power sample was washed with DMF (30 ml) and collected by centrifugation at 8000 rpm for 15 mins. The sample was then further washed with methanol (30 ml) for two times. The collected powders were dried under vacuum at 150 °C for 24 hrs.

Fabrication of UiO-66-NH$_2$ membranes

UiO-66-NH$_2$ membrane was synthesized solvothermally by an *in-situ* synthesis method. A metal solution was prepared by mixing 0.471 g of ZrCl$_4$ in 15 ml of DMF followed by solvothermal treatment at 120 °C for 2 hrs in a Teflon-lined autoclave. For a ligand solution, 0.364 g of H$_2$BDC-NH$_2$ was dissolved in 15 ml of DMF, followed by addition of 0.014 g of H$_2$O and 6.98 g of acetic acid. The ligand solution was poured into a Teflon-lined autoclave containing the metal solution. The solution was thoroughly mixed by magnetic stirring. An α-alumina disk was loaded vertically on a custom-made Teflon holder and then was placed in the mixture solution. Immediately after, the autoclave was heated at 180 °C for 24 hrs in a convection oven. The autoclave was cooled down at room temperature for 2 hrs. The membrane sample was washed with DMF overnight and further washed with methanol for 24 hrs at room temperature on a lab shaker. It was replenished with fresh methanol every 12 hrs. The membrane was dried at room temperature for 2 hrs and then activated at 150 °C under vacuum for 24 hrs.

Encapsulation of IL in UiO-66-NH$_2$ particles and membranes

An equimolar mixture of 1-MIM and C$_4$Br were used to synthesize [C$_4$MIM][Br]. First, UiO-66-NH$_2$ powders or membranes were saturated with 1-MIM by stirring for 24 hrs at room temperature. C$_4$Br was then added and continuously stirred for 48 hrs at room temperature. The sample was washed with methanol (30 ml) two times. The sample was dried at 80 °C under vacuum for 24 hrs.

Fabrication of supported IL membranes (SILMs)

Anodized alumina membranes (Anodisc 25, Whatman) with pore diameter of 20 nm were used as supports for [C$_4$MIM][Br] membranes. [C$_4$MIM][Br] was impregnated into an anodisc membrane by immersing the membrane in the liquid state IL overnight at room temperature. The prepared SILM was rinsed
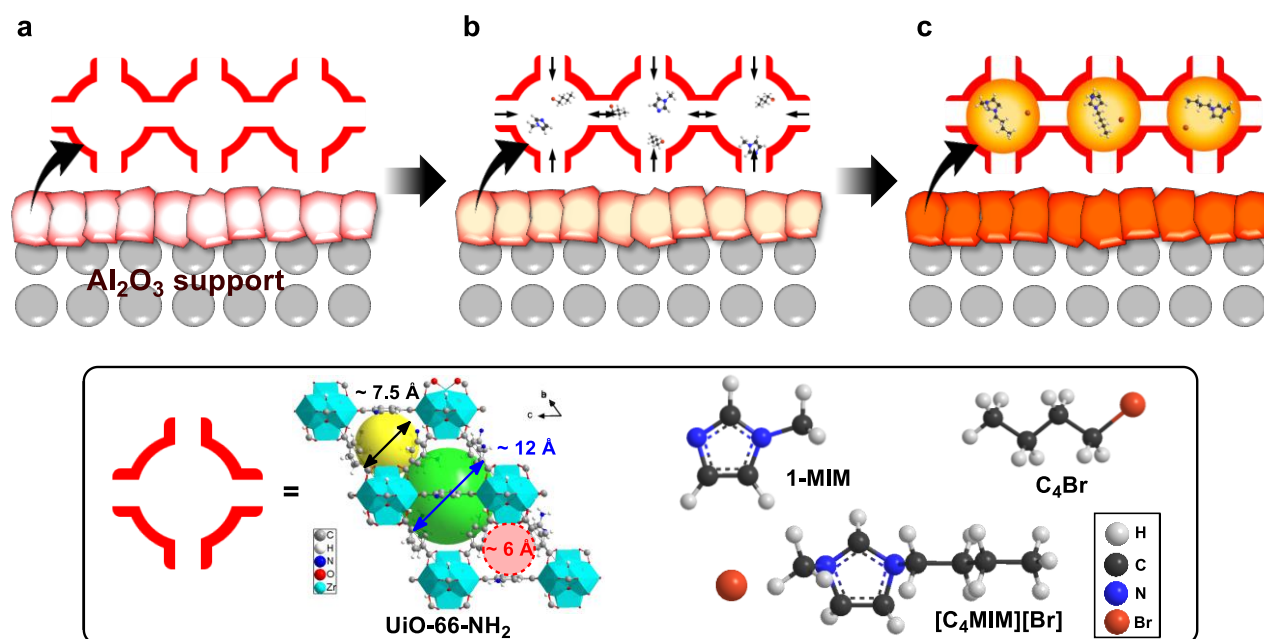
Fig. 1. Scheme of encapsulated ionic liquid membrane (EILM) preparation.

with methanol and gently blotted by a Kimwipe. The SILM was supported on a PVDF membrane (Durapore® Membrane filter 0.1 μl, EDM Millipore) to prevent the IL from leaching out.

Characterizations

X-ray diffraction (XRD) patterns were taken at a 2 ϑ range of 5 – 40 ° with Cu-Kα radiation (λ = 1.5406 Å) using an X-ray diffractometer (Rigaku Miniflex II). Scanning electron microscope (SEM, JEOL JSM-7500F) was used to investigate the morphology of samples at working distance of 15 mm and acceleration voltage of 5 keV. Water droplet contact angle measurement was carried out using a fixed volume of water droplet of 5 μl at room temperature. Images were taken using a microscope camera (Motic Moticam 1000) and analyzed by using ImageJ software. Thermogravimetric analysis (TGA, TA instruments Q50) was performed at a temperature range of 25 – 700 °C with a ramping rate of 10°C/min under air flow of 50 cm³ min⁻¹. For membrane samples, the weight of the substrates was subtracted after measurements. Solution proton nuclear magnetic resonance (¹H NMR) spectra were taken using Bruker Avance III (400 MHz system). NMR samples were prepared by dissolving in 40 μl D₂SO4-d2 followed by adding 560 μl DMF-d7. Isothermal N₂ and water vapor physisorption measurements were performed using ASAP 2020 plus (Micromeritics) at 77.3 K (-195.85 °C) and 293 K (20 °C), respectively. Heat of sorption of water vapor was determined by measuring water sorption at three different temperatures (20 °C, 30 °C, and 40 °C) and absolute pressure of 1.15 kPa. Kinetic water vapor sorption measurements were conducted with sample loadings of ~ 0.1 g at 20 °C and at p/p_o = 0.5 using ASAP 2020 plus (Micromeritics) using a ROA (rate of adsorption) software.

Permeation measurements

H₂O/N₂ separation performances of membranes were tested using a custom-made permeation system shown in Fig. S1. A humid feed stream was provided by adjusting the ratio of dry N₂ flow rate and water vapor saturated N₂ flow rate. The total flow rates were maintained at 200 cm³ min⁻¹ by mass flow controllers (MFC, DFC, AALBORG). The feed pressure was adjusted using a back-pressure regulator at the pressure range of 1.5-3.5 bar. The relative humidity was determined by a dew point meter (HMP7, Vaisala) and was kept at > 95 %. The permeate side was swept by an argon purge with a flow rate of 100 cm³ min⁻¹. The permeate side pressure was maintained at ~ 0.02 bar using a diaphragm pump (N 820.3 FTP, KNF). The compositions of the permeate side were determined using a gas analyzer (QGA, Hiden Analytical). The permeance of component i (P_i) was calculated using the following equation:[30]

$$P_i = \frac{\dot{n}_p \times x_{p,i}}{A(p_f \times x_{f,i} - p_p \times x_{p,i})}$$

where, $\dot{n}$ is the total flow rates, x_i is the mole fractions of component i, A is the area of membranes, p is the pressure, and the subscripts p and f are permeate side and feed side, respectively. The separation factor (α_{ij}) was obtained the equation below;

$$\alpha_{ij} = \frac{x_{p,i}/x_{p,j}}{x_{f,i}/x_{f,j}}$$

Results and discussion

Fabrication and characterizations of EILMs

Fig. 1 illustrates the preparation of EILMs by *in-situ* synthesizing IL, [C₄MIM][Br], in the cages of a polycrystalline UiO-66-NH₂ membrane via a SIB method. UiO-66-NH₂ was selected due to its stability in water vapor and hydrophilicity as well as its processability into polycrystalline membranes.[31] First, a UiO-66-
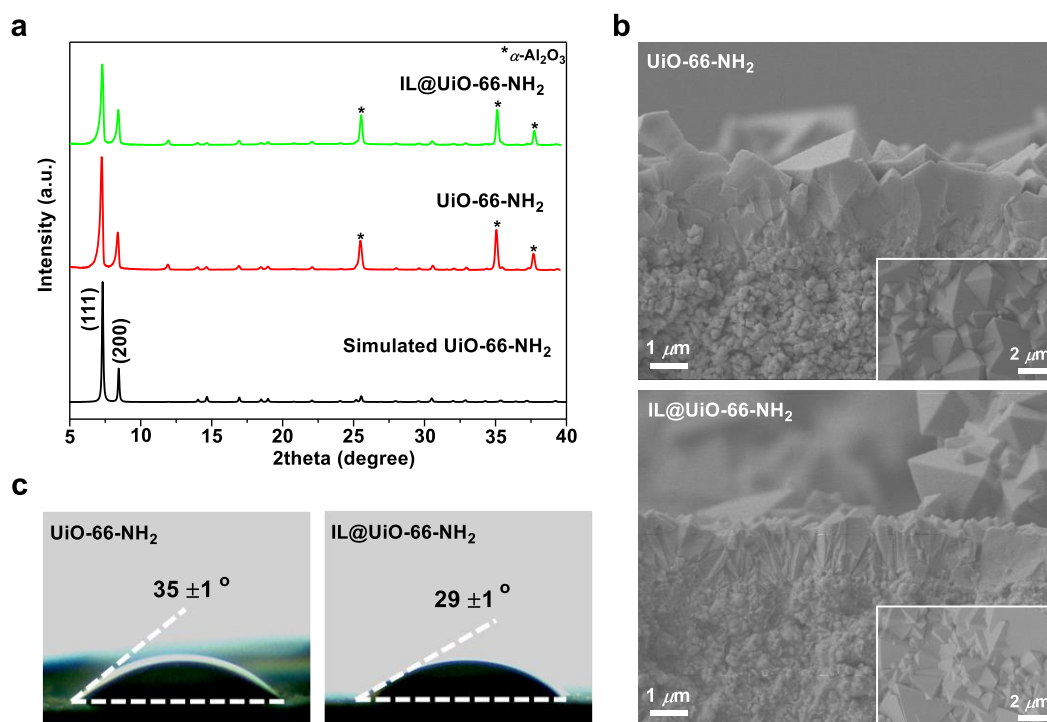
Fig. 2. (a) XRD patterns, (b) SEM images, and (c) water contact angles of UiO-66-NH$_2$ and IL@UiO-66-NH$_2$ membranes.

NH$_2$ membrane was fabricated solvothermally on an α-alumina disk by an *in-situ* method (Fig. 1a). It is noted that there have been only two reports on the synthesis of UiO-66-NH$_2$ membranes,[32, 33] both of which required modification of substrates in order to obtain intergrown membranes. In contrast, the membrane was prepared without substrate modification. Instead, we increased both precursor concentrations (both metal and ligand) and reaction temperature, promoting the intergrowth of UiO-66-NH$_2$ crystals. The UiO-66-NH$_2$ membrane was then saturated with 1-MIM followed by addition of C$_4$Br (Fig. 1b). When these two precursors were reacted, [C$_4$MIM][Br] IL was formed in the cages of the UiO-66-NH$_2$ framework. While the precursor molecules can freely diffuse through the 3-dimensionally microporous channels in the framework, the bulkier IL can be trapped in the cages, forming a [C$_4$MIM][Br]@UiO-66-NH$_2$ membrane (hereafter, IL@UiO-66-NH$_2$ membrane) (Fig. 1c). To form EILMs via a SIB method, it is of critical importance to properly match microporous membranes and ILs. That is to say, IL precursors should penetrate through the ultramicroporous apertures of membranes and yet IL, once formed, should be trapped inside the pore cages.[22, 34] UiO-66-NH$_2$ possesses two different cages, tetrahedral and octahedral ones with the diameters of ~ 7.5 Å and ~ 12 Å, respectively, that are interconnected with ~ 6 Å apertures (Fig. 1).[31] The size of [C$_4$MIM][Br] was estimated ~ 6 - 10 Å by the Connolly surface method (Fig. S2),[35] similar to the diameter obtained from the group contribution method (i.e., ~ 8 Å).[36] As such, it can be said that UiO-66-NH$_2$ has suitable sizes of apertures and cages to properly encapsulate the IL (i.e., 1-MIM & C$_4$Br < aperture of UiO-66-NH$_2$ < [C$_4$MIM][Br] ≈ tetrahedral cage of UiO-66-NH$_2$ < octahedral cage of UiO-66-NH$_2$). In addition, considering the

fact that the same IL was formed in ZIF-8 and NaY zeolite by SIB strategies,[34, 37] it was inferred that the IL precursors were able to readily pass through the apertures of UiO-66-NH$_2$.

Fig. 2a presents the XRD patterns of both UiO-66-NH$_2$ and IL@UiO-66-NH$_2$ membranes in comparison with a simulated pattern of UiO-66-NH$_2$ powder. The diffraction pattern of the UiO-66-NH$_2$ membrane matched well with the simulated one, confirming formation of a phase-pure UiO-66-NH$_2$ layer on an alumina support (Fig. 2a). Upon encapsulation of [C$_4$MIM][Br], the XRD of the IL@UiO-66-NH$_2$ membrane showed preservation of all peaks, indicating that there was no compromise in the crystal structure of UiO-66-NH$_2$. Nevertheless, the intensity of the (111) plane was decreased by around a third. As shown in Fig. S3, the (111) lattice planes are parallel to open triangular apertures surrounding octahedral cages where the encapsulated IL molecules are likely present, thereby leading to the compromise in the diffraction. Fig. 2b presents SEM images showing that UiO-66-NH$_2$ membranes appeared well-intergrown and defect-free (Fig. 2b top). No crack formation was observed on the membrane upon the IL impregnation (Fig. 2b bottom). As expected, the thickness of the membrane remained unchanged at ~ 2 μm. If confirmed the IL@UiO-66-NH$_2$ membranes would be one of the thinnest IL membranes reportred.[9, 38] Fig. 2c presents water contact angles before and after IL encapsulation. The contact angle decreased upon IL encapsulation, suggesting the presence of hydrophilic [C$_4$MIM][Br] on the external surface of the EILM.

Quantity analysis of IL encapsulated

Table 1 summarizes the quantity of [C$_4$MIM][Br] encapsulated in EILMs determined by three different bases (i.e., weight, volume, and mole ratio). According to TGA analysis (Fig. S4), the
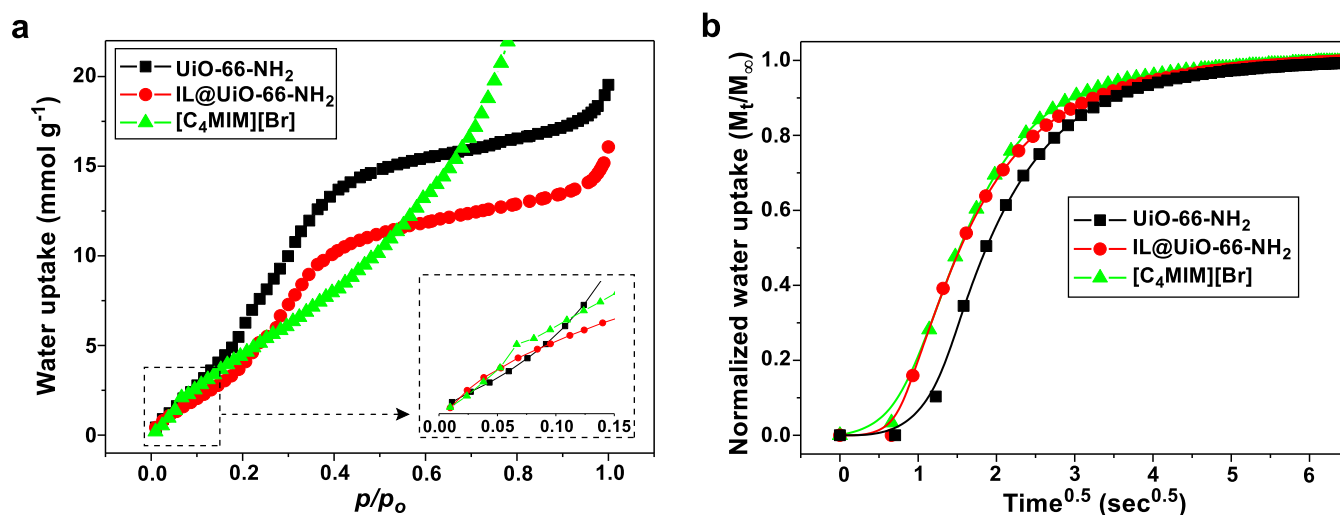
Fig. 3. (a) Water vapor absorption isotherms at 20 °C and (b) uptake kinetics of water vapor at 20 °C and p/p_o = 0.5 with the first aliquot dosing. The insert in (a) shows magnified isotherms in the range of p/p_o = 0.00 − 0.15. For clarity, the water update isotherm of IL was cut at p/p_o ~ 0.78 due to its exceptionally high uptake as compared to the other samples.

residual weight of the UiO-66-NH$_2$ membrane was 40.7 wt%, which was comparable but slightly lower than the theoretical residual weight of 43.2 wt% possibly due to the absorbed moisture. The theoretical residual weight was determined by assuming that there were no defects in UiO-66-NH$_2$ crystals and all Zr atoms turned into ZrO$_2$ upon thermal oxidization. As expected, the IL@UiO-66-NH$_2$ membrane exhibited greater weight loss upon thermal oxidation than the UiO-66-NH$_2$ membrane due to the decomposition of the encapsulated [C$_4$MIM][Br] (Fig. S4). Based on the difference in the residual weights of the two membranes, the loading percentage of IL (i.e., the mass of IL encapsulated divided by the mass of IL@UiO-66-NH$_2$) was estimated ~ 19.5 wt%.[39] It should be mentioned that the residual weight of an IL@UiO-66-NH$_2$ powder sample was consistent with that of an IL@UiO-66-NH$_2$ membrane sample (see Fig. S5). Hence, the other two quantitative analysis (i.e., volume and mole ratio) were conducted on powder samples (Fig. S6).

For volume-based quantification, N$_2$ adsorption isotherms were taken on UiO-66-NH$_2$ and IL@UiO-66-NH$_2$ powder samples. Both showed a type-I isotherm (Fig. S7), whereas [C$_4$MIM][Br] showed only negligible N$_2$ adsorption (i.e., type-III). As can be seen in the isotherms, the pore volume of UiO-66-NH$_2$ was reduced to ~ 36.5 % upon IL encapsulation (Table 1). This means that ~ 36.5 vol% of the total pore volume of UiO-66-NH$_2$ was filled with IL. If some cages are filled with the IL, penetrant precursor molecules are likely to have limited accessibility to other cages. It is, therefore, expected that there exists an optimal IL loading.

Lastly, [C$_4$MIM][Br] encapsulated was quantified by determining the molar ratio of UiO-66-NH$_2$ ligand (i.e., H$_2$BDC-NH$_2$) and [C$_4$MIM][Br] using ^{1}H NMR analysis. As presented in Fig. S8, the peaks corresponding to [C$_4$MIM][Br] were found in the IL@UiO-66-NH$_2$, demonstrating the encapsulation of the IL in the UiO-66-NH$_2$. The molar ratio of H$_2$BDC-NH$_2$ and [C$_4$MIM][Br] was estimated ~ 4.1 (Table 1). Since there are 24 ligands per unit cell, about 5.9 [C$_4$MIM][Br] molecules were

encapsulated per unit cell. Based on the molar ratio and the molecular weights of UiO-66-NH$_2$ and [C$_4$MIM][Br] (i.e., 6848.1 and 219.1 g mol^{-1}, respectively), the IL loading percentage was back-calculated ~ 15.9 wt%, which is comparable to the TGA result of ~ 19.5 wt%. There are four tetrahedral and four octahedral cages in unit cell (Fig. S9), resulting in the volume of the cages of ~ 4502.8 A^3 in a unit cell. Give the molecular volume of [C$_4$MIM][Br] obtained from the group contribution method (i.e., 285 A^3),[36] it was determined that ~ 37.3 % of the cage volume was filled by IL molecules, which was consistent with the N$_2$ physisorption result of ~ 36.5 %.

Table 1. Quantification of encapsulated [C$_4$MIM][Br] in UiO-66-NH$_2$.

Sample	Residual weight (wt%)[a]	Pore volume (cm^3 g^{-1})[b]	Molar ratio of H$_2$BDC-NH$_2$/[C$_4$MIM][Br][b]
UiO-66-NH$_2$	40.7 ± 1.3	0.351 ± 0.008	n/a
IL@UiO-66-NH$_2$	35.6 ± 0.6	0.223 ± 0.005	4.1 ± 1.6

a Membrane samples. b Powder samples.

Sorption and diffusion of water vapor

Fig. 3 presents water uptake and uptake kinetics of UiO-66-NH$_2$, [C$_4$MIM][Br], and IL@UiO-66-NH$_2$. It is reminded that the measurements were performed on powder samples of UiO-66-NH$_2$ and IL@UiO-66-NH$_2$. As can be seen in Fig. 3a, both UiO-66-NH$_2$ and IL@UiO-66-NH$_2$ exhibited Langmuir-type isotherms while [C$_4$MIM][Br] showed a linear isotherm following Henry's law. These observations are consistent with the fact that UiO-66-NH$_2$ and IL@UiO-66-NH$_2$ are microporous solids while [C$_4$MIM][Br] is a dense liquid. IL@UiO-66-NH$_2$ showed lower adsorption than UiO-66-NH$_2$ because of its lower micropore volume resulting from IL encapsulation (see Table 1). At the low relative pressure range, UiO-66-NH$_2$ displayed a concave curve while IL@UiO-66-NH$_2$ showed a convex curve (see the insert in
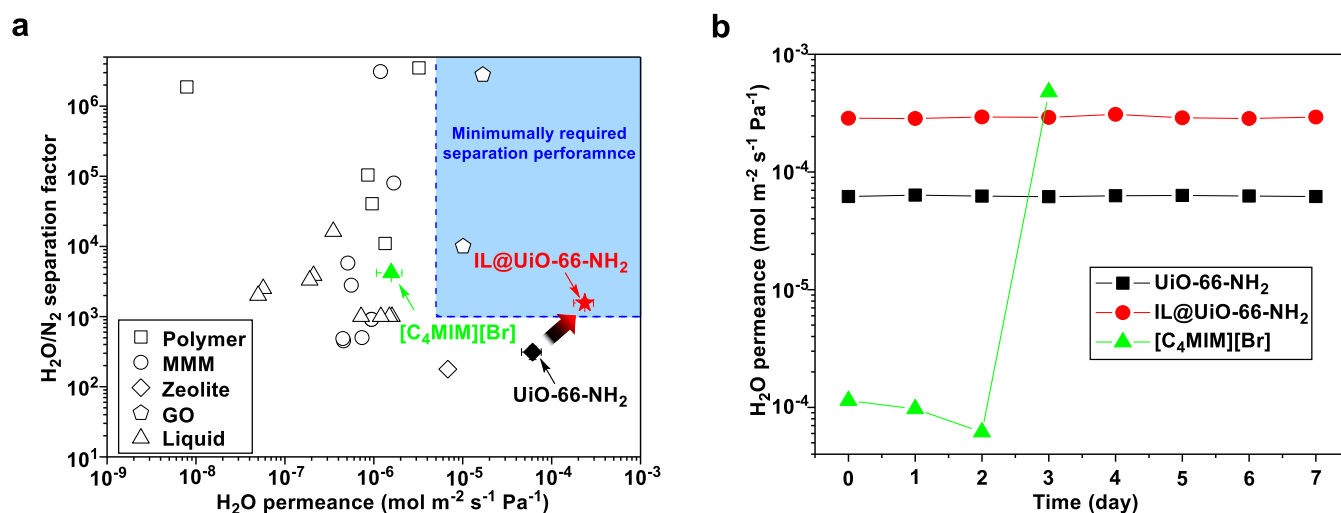
Fig. 4. (a) H_2O/N_2 separation performance of the EILMs compared with those reported in literatures[5-7, 30, 43-55] and (b) time-dependent H_2O permeances at 20 °C and 1.5 bar of feed pressure.

Fig. 3a). This implies that IL@UiO-66-NH$_2$ exhibited enhanced interaction with water upon the encapsulation of [C$_4$MIM][Br],[40] which was corroborated with the fact that the heat of sorption of IL@UiO-66-NH$_2$ (-54.13 kJ mol^{-1}) was lower than that of UiO-66-NH$_2$ (-51.76 kJ mol^{-1}) (Table S1). It is noted that [C$_4$MIM][Br] showed the highest heat of sorption (-40.01 kJ mol^{-1}), suggesting water molecules in bulk IL were energetically less favorable than those in the microporous frameworks (Table S1).[41]

The kinetics of water vapor adsorption of IL@UiO-66-NH$_2$ was found greater than that of UiO-66-NH$_2$ upon dosing the first aliquot (Fig. 3b). This increase was likely due to the presence of encapsulated [C$_4$MIM][Br]. It is noteworthy of mentioning that [C$_4$MIM][Br] showed the fastest water vapor adsorption among the samples (see Fig. 3b). Pertaining to the non-steady state initial sorption rate (i.e., linear region up to 0.5 of the equilibrium values), it was possible to calculate the effective diffusion coefficients (D_{eff}) graphically using the sorption-time curves (Table S2). The detailed calculation is represented in the Supporting Information. The D_{eff} values increased by the following orders: 4.91 x 10^{-11} cm^2 s^{-1} for UiO-66-NH$_2$ < 6.01 x 10^{-11} cm^2 s^{-1} for IL@UiO-66-NH$_2$ < 2.22 x 10^{-7} cm^2 s^{-1} for [C$_4$MIM][Br]. The D_{eff} of IL@UiO-66-NH$_2$ was ~ 22 % greater than that of UiO-66-NH$_2$, whereas that of [C$_4$MIM][Br] was four orders of magnitude higher than the other two.[42] For overall dosing, however, the absorption rate of bulk [C$_4$MIM][Br] was significantly lower than those of UiO-66-NH$_2$ and IL@UiO-66-NH$_2$ (Fig. S10). For the first aliquot dosing, the sorption of water in bulk [C$_4$MIM][Br] occurs mainly at the air/IL interface. However, once the interfacial region is saturated, water molecules may need to penetrate deeper into bulk IL, consequently decreasing the overall adsorption kinetics. For the overall dosing, the water diffusion of IL@UiO-66-NH$_2$ was still faster than that of UiO-66-NH$_2$ (Fig. S10). This reveals that encapsulated [C$_4$MIM][Br] was considerably more efficient than bulk [C$_4$MIM][Br] due to the increased contact surface area of IL with water molecules. Furthermore, the viscosity effect of [C4MIM][Br], which plays a significant role in a bulk phase,

might be negligible since [C4MIM][Br] is dispersed in the cages at a molecular level, thereby IL@UiO-66-NH$_2$ showing enhanced the diffusion of water vapor as compared to [C$_4$MIM][Br].

H$_2$O/N$_2$ separation performances of EILMs and their stability

The H$_2$O/N$_2$ separation performances of EILMs were evaluated by comparing with the previously reported air-dehumidification membranes (Fig. 4a and Table S3).[5-7, 30, 43-55] It turned out that there were a couple of studies reported on the minimally required H$_2$O/N$_2$ separation performances of membranes for energy effective air-dehumidification.[56, 57] According to those studies,[56, 57] the water permeance should be at least 5 x 10^{-6} mol m^{-2} s^{-1} Pa^{-1} (i.e., 14,900 GPU) and the required H$_2$O/N$_2$ selectivity ought to be 1000 and greater (Fig. 4a). There were, however, only a few graphene-oxide (GO) membranes that satisfied the criterial so far.[54, 55] Surprisingly, the IL@UiO-66-NH$_2$ membranes met the criterial under mixed gas conditions while both UiO-66-NH$_2$ and [C$_4$MIM][Br] membranes failed to meet the criteria (Fig. 4a). In particular, the IL@UiO-66-NH$_2$ membranes showed the average H$_2$O permeance of 2.36 x 10^{-4} mol m^{-2} s^{-1} Pa^{-1} which is, to the best of our knowledge, the highest H$_2$O permeance ever reported (Fig. 4a). This exceptionally high H$_2$O permeance can be attributed to the ultrathin nature of the membrane as well as to the enhanced efficiency of encapsulated [C$_4$MIM][Br]. Meanwhile, the H$_2$O permeance of the [C$_4$MIM][Br] membranes (i.e., supported IL membrane) was as low as other supported liquid membranes reported owing to its lower efficiency as well as its greater thickness.[5-7] As compared to the UiO-66-NH$_2$ membranes, the IL@UiO-66-NH$_2$ membranes exhibited much enhanced H$_2$O/N$_2$ separation factor (~1564 vs. ~312) due to the presence of the highly water selective [C$_4$MIM][Br] (note that the H$_2$O/N$_2$ separation factor of the IL was ~ 4206).

Stability of membrane is important for the practical applications. As shown in Fig. 4b, the H$_2$O permeance of both UiO-66-NH$_2$ and IL@UiO-66-NH$_2$ membranes were well-maintained during 7 days of operation. However, the [C$_4$MIM][Br] liquid membrane showed unstable H$_2$O permeability with time (Fig. 4b). After a couple of days, the H$_2$O permeability of the [C$_4$MIM][Br] membrane decreased and then

suddenly increased sharply. Typically, ILs were immobilized in supports by a high capillary force and a high viscosity.[58] As such, the stability of supported IL membranes is greatly affected by the properties of both ILs and supports. The unstable performance of the [C$_4$MIM][Br] membrane is likely due to its relatively low viscosity and high solubility with the water vapor of the feed stream.[59] As water content in [C$_4$MIM][Br] increased upon extended operation, viscosity of [C4MIM][Br] was likely further reduced,[60] thereby leading to leaching of [C$_4$MIM][Br] from the support.[10] On the other hand, [C$_4$MIM][Br] was trapped in the cages of the UiO-66-NH$_2$ membranes, making it difficult for the IL to leach out even under the high humidity conditions. As a consequence, the EILM showed stable separation performance over 7 days of operation. The stability of the IL membranes under various conditions was also tested. At the higher feed pressure and temperature, the IL@UiO-66-NH$_2$ showed significantly improved separation performances compared to [C$_4$MIM][Br] membranes (Fig. S11 and S12).

Conclusions

In conclusion, we successfully formed the encapsulated ionic liquid membranes (EILMs) by encapsulating [C$_4$MIM][Br] in polycrystalline UiO-66-NH$_2$ MOF membranes via a ship-in-a-bottle method. The resulting EILMs (i.e., [C$_4$MIM][Br]@UiO-66-NH$_2$ membranes) were ~ 2 μm thick, one of the thinnest IL membranes reported. It was found that the loading percentage of the encapsulated [C$_4$MIM][Br] was ~19.5 wt% , occupying ~ 36.5 vol% of the total cage volume of UiO-66-NH$_2$. Although the IL-encapsulated UiO-66-NH$_2$ membranes showed slightly lower water vapor uptake due to their reduced free pore volume, they showed greater affinity to water vapor than as-prepared UiO-66-NH$_2$ owing to the presence of the hydrophilic IL. The IL@UiO-66-NH$_2$ membranes showed increased water vapor uptake kinetics, thereby enhancing H$_2$O permeance. The EILMs exhibited the highest H$_2$O permeance among air-dehumidification membranes reported due to 1) enhanced IL efficiency upon encapsulation and 2) ultrathin nature of the microporous framework membranes. Furthermore, encapsulation of the IL substantially increased the H$_2$O/N$_2$ separation factor of the membranes from ~ 312 to ~ 1564. Finally, the EILMs displayed noticeably enhanced stability for H$_2$O/N$_2$ separation as compared with the [C$_4$MIM][Br] SILMs under various operation conditions. The current EILMs are expected a major step forward in the development of practical air-dehumidification membranes for energy-efficient HVAC systems.

Conflicts of interest

There are no conflicts to declare.

Acknowledgements

References

1. P. D. H. John J. Conti, James, S. A. N. R. Diefenderfer, A., J. Michael Schaal, L. D. T. Turnure and Westfall, *Annual Energy Outlook 2014*, U.S. Energy Information Administration (EIA), Washington, DC, 2014.
2. M. F. Lunt, M. Rigby, A. L. Ganesan, A. J. Manning, R. G. Prinn, S. O'Doherty, J. Muhle, C. M. Harth, P. K. Salameh, T. Arnold, R. F. Weiss, T. Saito, Y. Yokouchi, P. B. Krummel, L. P. Steele, P. J. Fraser, S. L. Li, S. Park, S. Reimann, M. K. Vollmer, C. Lunder, O. Hermansen, N. Schmidbauer, M. Maione, J. Arduini, D. Young and P. G. Simmonds, *P Natl Acad Sci USA*, 2015, **112**, 5927-5931.
3. R. Z. William Goetzler, Jim Young, Caitlin Johnson, *Energy Savings Potential and RD&D Opportunities for Non-Vapor-Compression HVAC Technologies*, U.S. Department of Energy, 2014.
4. H. T. El-Dessouky, H. M. Ettouney and W. Bouhamra, *Chem Eng Res Des*, 2000, **78**, 999-1009.
5. A. Ito, *J Membr Sci*, 2000, **175**, 35-42.
6. P. Scovazzo, *J Membr Sci*, 2010, **355**, 7-17.
7. A. Kudasheva, T. Kamiya, Y. Hirota and A. Ito, *J Membr Sci*, 2016, **499**, 379-385.
8. M. Qu, O. Abdelaziz, Z. M. Gao and H. X. Yin, *Renew Sust Energ Rev*, 2018, **82**, 4060-4069.
9. L. J. Lozano, C. Godínez, A. P. de los Ríos, F. J. Hernández-Fernández, S. Sánchez-Segado and F. J. Alguacil, *J Membr Sci*, 2011, **376**, 1-14.
10. W. Zhao, G. H. He, F. Nie, L. L. Zhang, H. C. Feng and H. J. Liu, *J Membr Sci*, 2012, **411**, 73-80.
11. M. A. Malik, M. A. Hashim and F. Nabi, *Chem Eng J*, 2011, **171**, 242-254.
12. M. E. Perez-Blanco and E. J. Maginn, *J Phys Chem B*, 2010, **114**, 11827-11837.
13. B. Sasikumar, G. Arthanareeswaran and A. F. Ismail, *J Mol Liq*, 2018, **266**, 330-341.
14. H. Gao, L. Bai, J. Han, B. Yang, S. Zhang and X. Zhang, *Chem Commun*, 2018, **54**, 12671-12685.
15. J. E. Bara, S. Lessmann, C. J. Gabriel, E. S. Hatakeyama, R. D. Noble and D. L. Gin, *Ind Eng Chem Res*, 2007, **46**, 5397-5404.
16. B. A. Voss, J. E. Bara, D. L. Gin and R. D. Noble, *Chem Mater*, 2009, **21**, 3027-3029.
17. K. Friess, J. C. Jansen, F. Bazzarelli, P. Izák, V. Jarmarová, M. Kačírková, J. Schauer, G. Clarizia and P. Bernardo, *J Membr Sci*, 2012, **415-416**, 801-809.
18. S. Zhang, J. Zhang, Y. Zhang and Y. Deng, *Chem Rev*, 2017, **117**, 6755-6833.
19. F. P. Kinik, A. Uzun and S. Keskin, *ChemSusChem*, 2017, **10**, 2842-2863.

20. K. Fujie and H. Kitagawa, *Coordin Chem Rev*, 2016, **307**, 382-390.

21. Q.-x. Luo, M. Ji, M.-h. Lu, C. Hao, J.-s. Qiu and Y.-q. Li, *J Mater Chem A*, 2013, **1**, 6530-6534.

22. N. A. Khan, Z. Hasan and S. H. Jhung, *Chem Commun*, 2016, **52**, 2561-2564.

23. Z. Li, W. Wang, Y. Chen, C. Xiong, G. He, Y. Cao, H. Wu, M. D. Guiver and Z. Jiang, *J Mater Chem A*, 2016, **4**, 2340-2348.

24. N. A. Khan, Z. Hasan and S. H. Jhung, *Chem-Eur J*, 2014, **20**, 376-380.

25. L. Hao, P. Li, T. Yang and T.-S. Chung, *J Membr Sci*, 2013, **436**, 221-231.

26. Y. J. Ban, Z. J. Li, Y. S. Li, Y. Peng, H. Jin, W. M. Jiao, A. Guo, P. Wang, Q. Y. Yang, C. L. Zhong and W. S. Yang, *Angew Chem Int Edit*, 2015, **54**, 15483-15487.

27. J. Ma, Y. Ying, X. Guo, H. Huang, D. Liu and C. Zhong, *J Mater Chem A*, 2016, **4**, 7281-7288.

28. H. T. Kwon and H.-K. Jeong, *Chem Commun*, 2013, **49**, 3854-3856.

29. F. Wu, L. Lin, H. Liu, H. Wang, J. Qiu and X. Zhang, *J Membr Sci*, 2017, **544**, 342-350.

30. R. Xing, Y. X. Rao, W. TeGrotenhuis, N. Canfield, F. Zheng, D. W. Winiarski and W. Liu, *Chem Eng Sci*, 2013, **104**, 596-609.

31. P. M. Schoenecker, C. G. Carson, H. Jasuja, C. J. J. Flemming and K. S. Walton, *Ind Eng Chem Res*, 2012, **51**, 6513-6519.

32. L. Wan, C. Zhou, K. Xu, B. Feng and A. Huang, *Micropor Mesopor Mat*, 2017, **252**, 207-213.

33. F. Wu, Y. Cao, H. Liu and X. Zhang, *J Membr Sci*, 2018, **556**, 54-65.

34. Y. Yu, J. Mai, L. Wang, X. Li, Z. Jiang and F. Wang, *Sci Rep-Uk*, 2014, **4**, 5997-6004.

35. M. L. Connolly, *J Appl Crystallogr*, 1983, **16**, 548-558.

36. R. L. Gardas and J. A. P. Coutinho, *Fluid Phase Equilibr*, 2008, **266**, 195-201.

37. I. Ahmed, T. Panja, N. A. Khan, M. Sarker, J.-S. Yu and S. H. Jhung, *Acs Appl Mater Inter*, 2017, **9**, 10276-10285.

38. P. T. Nguyen, B. A. Voss, E. F. Wiesenauer, D. L. Gin and R. D. Nobe, *Ind Eng Chem Res*, 2013, **52**, 8812-8821.

39. S. H. Shen, Y. S. Wu, Y. C. Liu and D. C. Wu, *Int J Nanomed*, 2017, **12**, 4085-4109.

40. S. Brunauer, L. S. Deming, W. E. Deming and E. Teller, *J Am Chem Soc*, 1940, **62**, 1723-1732.

41. A. Deyko and R. G. Jones, *Faraday Discuss*, 2012, **154**, 265-288.

42. M. A. Rocha and M. B. Shiflett, *Ind Eng Chem Res*, 2019, **58**, 1743-1753.

43. S. J. Metz, W. J. C. van de Ven, J. Potreck, M. H. V. Mulder and M. Wessling, *J Membr Sci*, 2005, **251**, 29-41.

44. S. M. Allen, M. Fujii, V. Stannett, H. B. Hopfenberg and J. L. Williams, *J Membr Sci*, 1977, **2**, 153-163.

45. H. Sijbesma, K. Nymeijer, R. van Marwijk, R. Heijboer, J. Potreck and M. Wessling, *J Membr Sci*, 2008, **313**, 263-276.

46. T. Puspasari, F. H. Akhtar, W. Ogieglo, O. Alharbi and K. V. Peinemann, *J Mater Chem A*, 2018, **6**, 9271-9279.

47. T. D. Bui, F. Chen, A. Nida, K. J. Chua and K. C. Ng, *Sep Purif Technol*, 2015, **144**, 114-122.

48. D. T. Bui, A. Nida, K. C. Ng and K. J. Chua, *J Membr Sci*, 2016, **498**, 254-262.

49. F. H. Akhtar, M. Kumar and K.-V. Peinemann, *J Membr Sci*, 2017, **525**, 187-194.

50. M. I. Baig, P. G. Ingole, W. K. Choi, J. D. Jeon, B. Jang, J. H. Moon and H. K. Lee, *Chem Eng J*, 2017, **308**, 27-39.

51. M. I. Baig, P. G. Ingole, W. K. Choi, S. R. Park, E. C. Kang and H. K. Lee, *J Membr Sci*, 2016, **514**, 622-635.

52. P. G. Ingole, R. R. Pawar, M. I. Baig, J. D. Jeon and H. K. Lee, *J Mater Chem A*, 2017, **5**, 20947-20958.

53. M. I. Baig, P. G. Ingole, J.-d. Jeon, S. U. Hong, W. K. Choi and H. K. Lee, *Chem Eng J*, 2019, **373**, 1190-1202.

54. Y. Shin, W. Liu, B. Schwenzer, S. Manandhar, D. Chase-Woods, M. H. Engelhard, R. Devanathan, L. S. Fifield, W. D. Bennett, B. Ginovska and D. W. Gotthold, *Carbon*, 2016, **106**, 164-170.

55. W. S. Hung, Y. L. Lai, P. H. Lee, Y. H. Chiao, A. Sengupta, M. Sivakumar, K. R. Lee and J. Y. Lai, *Sep Purif Technol*, 2020, **239**, 116499-116506.

56. O. Tanskyi, PhD, Texas A & M University, 2015.

57. T. D. Bui, Y. Wong, M. R. Islam and K. J. Chua, *J Membr Sci*, 2017, **539**, 76-87.

58. D. Hopkinson, M. Zeh and D. Luebke, *J Membr Sci*, 2014, **468**, 155-162.

59. Y. Y. Cao, Y. Chen, X. F. Sun, Z. M. Zhang and T. C. Mu, *Phys Chem Chem Phys*, 2012, **14**, 12252-12262.

60. F. J. Hernandez-Fernandez, A. P. de los Rios, F. Tomas-Alonso, J. M. Palacios and G. Villora, *J Membr Sci*, 2009, **341**, 172-177.